available at www.sciencedirect.com
journal homepage: www.europeanurology.com

European Association of Urology

Platinum Priority – Prostate Cancer

*Editorial by David A. Quigley on pp. 212–213 of this issue*

# Advanced Prostate Cancer with ATM Loss: PARP and ATR Inhibitors

*Antje Neeb [a,†], Nicolas Herranz [b,c,†], Sara Arce-Gallego [b,c,†], Susana Miranda [a], Lorenzo Buroni [a], Wei Yuan [a], Alejandro Athie [b], Teresa Casals [b], Juliet Carmichael [a,d], Daniel Nava Rodrigues [a], Bora Gurel [a], Pasquale Rescigno [a,d], Jan Rekowski [a], Jon Welti [a], Ruth Riisnaes [a], Veronica Gil [a], Jian Ning [a], Verena Wagner [e], Irene Casanova-Salas [b], Sarai Cordoba [b], Natalia Castro [b], Maria Dolores Fenor de la Maza [a,d], George Seed [a], Khobe Chandran [a,d], Ana Ferreira [a], Ines Figueiredo [a], Claudia Bertan [a], Diletta Bianchini [a,d], Caterina Aversa [a,d], Alec Paschalis [a,d], Macarena Gonzalez [b,f], Rafael Morales-Barrera [b,f], Cristina Suarez [b,f], Joan Carles [b,f], Amanda Swain [a], Adam Sharp [a,d], Jesus Gil [e], Violeta Serra [b,c], Christopher Lord [a], Suzanne Carreira [a,‡], Joaquin Mateo [b,f,‡,*], Johann S. de Bono [a,d,‡,*]*

[a] *The Institute of Cancer Research, London, UK;* [b] *Vall d'Hebron Institute of Oncology (VHIO), Barcelona, Spain;* [c] *Vall d'Hebron Institute of Research (VHIR), Barcelona, Spain;* [d] *The Royal Marsden NHS Foundation Trust, London, UK;* [e] *MRC London Institute of Medical Sciences (LMS) and Institute of Clinical Sciences (ICS), Faculty of Medicine, Imperial College, London, UK;* [f] *Vall d'Hebron University Hospital, Barcelona, Spain*

**Article info**

***Article history:***
Accepted October 18, 2020

***Associate Editor:***
T Morgan

***Keywords:***
Prostate cancer
ATM
DNA damage response
Synthetic lethality
PARP inhibition
ATR inhibition

**Abstract**

***Background:*** Deleterious ATM alterations are found in prostate cancer (PC) and associate with a higher grade; PARP inhibition has antitumour activity against this subset, but only some ATM loss PCs respond.
***Objective:*** To characterise ATM-deficient lethal PC and to study synthetic lethal therapeutic strategies for this subset.
***Design, setting, and participants:*** We studied advanced PC biopsies using validated immunohistochemical (IHC) and next-generation sequencing (NGS) assays.
***Outcome measurements and statistical analysis:*** In vitro cell line models modified using CRISPR-Cas9 to impair ATM function were generated and used in drug-sensitivity and functional assays, with validation in a patient-derived model.
***Results and limitations:*** Overall, we detected ATM IHC loss in 68/631 (11%) PC patients with synchronous and metachronous intrapatient heterogeneity; 45/61 (74%) of ATM loss tumours had *ATM* mutations or deletions by NGS. ATM IHC loss was not associated with worse outcome from advanced disease, but ATM loss was associated with increased genomic instability (the number of subchromosomal regions with allelic imbalance extending to the telomere, $p = 0.005$; large-scale transition, $p = 0.05$). In vitro, ATM loss PC models were sensitive to ATR inhibition, but had variable sensitivity to PARP

† Antje Neeb, Nicolas Herranz, and Sara Arce-Gallego contributed equally and are joint lead authors.
‡ Suzanne Carreira, Joaquin Mateo, and Johann S. de Bono are joint senior authors.
* Corresponding authors. The Institute of Cancer Research, 15 Cotswold Road, London SM2 5NG, UK. Tel. +44 208 722 4029; Fax: +44 208 642 7979 (J.S. de Bono). Clinical Research Program, Vall dHebron Institute of Oncology (VHIO), Vall dHebron University Hospital, 115-117 Natzaret, Cellex Center, 08035 Barcelona, Spain. Tel. +34 932543450 ext 8689 (J. Mateo).
E-mail addresses: jmateo@vhio.net (J. Mateo), Johann.debono@icr.ac.uk (J.S. de Bono).

https://doi.org/10.1016/j.eururo.2020.10.029


inhibition; superior antitumour activity was seen with combined PARP and ATR inhibition in these models.
***Conclusions:*** ATM loss in PC is not always detected by targeted NGS, associates with genomic instability, and is most sensitive to combined ATR and PARP inhibition.
***Patient summary:*** Of aggressive prostate cancers, 10% lose the DNA repair gene *ATM*; this loss may identify a distinct prostate cancer subtype that is most sensitive to oral drugs targeting both PARP and ATR.


## 1. Introduction

Metastatic castration-resistant prostate cancer (mCRPC) exhibits significant interpatient heterogeneity; molecular stratification is postulated to be key to improving outcomes [1–3]. PARP inhibition improves survival from mCRPC with DNA repair defects, leading to regulatory approval [4]. Patients with *BRCA2*-altered mCRPC derive most benefit [5,6], with only a minority of mCRPC with ATM mutations, comprising 5–10% of mCRPC [7–9], responding to PARP inhibition.

The ATM serine/threonine kinase is activated by DNA damage guarding cellular genomic stability [10] by activating DNA repair and regulating cell cycle checkpoints, senescence, and apoptosis [10,11]. ATM phosphorylates TopBP1 and promotes its interaction with ATR [12], which regulates replication initiation, prevents unregulated excessive cell replication, delays cell cycle progression, and stabilises DNA replication forks [13–15]. Inhibition of ATR induces replication stress and causes stalled replication forks that generate cytotoxic DNA double-strand breaks (DSBs). ATM restores replication fork topology and arrests cell cycle progression to permit repair. In ATM-deficient cells, this protective mechanism is absent, precipitating DNA damage, mitotic catastrophe, senescence, and/or cell death [16]. ATM loss can be synthetically lethal with ATR inhibition and may be a therapeutic strategy for ATM-deficient prostate cancer (PC) [17]. A first-in-human clinical trial of the ATR inhibitor BAY1895344 reported antitumour activity against cancers with ATM loss [18].

Herein, we study ATM loss by next-generation sequencing (NGS) and immunohistochemistry (IHC) in advanced PC, presenting data on PARP and ATR inhibitors alone and in combination in genetically manipulated and patient-derived models with ATM loss.

## 2. Patients and methods

### 2.1. Patient sample collection and processing

Samples were acquired using an approved protocol for PC molecular characterisation at the Royal Marsden (04/Q0801/60). All patients provided written informed consent. If more than one biopsy core for primary was available, the highest Gleason score lesion was used. Demographic and clinical data for each patient were collected retrospectively. Tissue blocks were reviewed by two pathologists (D.N.R. and B.G.).

### 2.2. Clinical data and statistical analysis

The ATM loss cohort was defined as patients with complete loss of ATM by IHC (H score 0). A previously reported subgroup (all included in this IHC study and with H score >0) [19] was used as control ($n = 88$); clinical outcome data included overall survival from PC diagnosis and from castration-resistant PC (CRPC), and the time from diagnosis to CRPC. For survival analyses, patients were censored at the date of last contact; for time to CRPC, there are no censored observations as all patients have become castrate resistant. Differences in these three endpoints based on ATM status were analysed using Kaplan-Meier curves and log-rank test. Univariable Cox regression models provided unadjusted hazard ratios as measures of effect size alongside their 95% confidence intervals (CIs). Data were analysed using R version 3.6.2 (R Foundation for Statistical Computing, Vienna, Austria).

### 2.3. ATM IHC

ATM protein expression was determined by IHC using a rabbit monoclonal anti-ATM antibody, clone Y170 (catalogue no. ab32420; Abcam Plc, Cambridge, UK), as described previously [20]. Detailed methods are described is in the Supplementary material.

### 2.4. Targeted and whole-exome sequencing

Genomic DNA was isolated using the QIAmp DNA FFPE Tissue kit (Qiagen) from tumour tissue sections (paired germline DNA was not analysed). Targeted sequencing libraries were constructed using a customised panel (Generead DNAseq Mix-n-Match Panel version 2; Qiagen) [5,21] and sequenced using a MiSeq Sequencer (Illumina). Whole-exome sequencing (WES) libraries were prepared using Kapa Hyper Plus Library Prep Kits and Agilent SureSelectXT V6 target enrichment kit. Paired-end sequencing was performed using the NovaSeq6000 S2 flow cell ($2 \times 100$ cycles; Illumina). MuTect2 was used for mutation calling; copy-number estimation was obtained through modified ASCAT2 package. Pathogenic germline mutations were also reviewed from WES data. Further details are provided in the Supplementary material. The number of subchromosomal regions with allelic imbalance extending to the telomere (NtAI) [22] and large-scale transitions (LSTs: chromosomal breaks between adjacent regions of at least 10 Mb) were assessed.

#### 2.4.1. Cell lines and culture

Cells were obtained from the LGC standards/ATCC, cultivated according to the supplier's recommendations, STR profiled, and tested regularly for mycoplasma. Media details are listed in Supplementary Table 1.

#### 2.4.2. CRISPR/Cas9 gene editing

The 22Rv.1 cells were transfected (TransIT-X2 reagent; Myrus) with 1 μg of an ATM Double Nickase Plasmid (sc-400192-NIC; Santa Cruz). Transfected cells were selected with 1 μg/ml puromycin (Thermo Fisher Scientific) for 4 d, and surviving cells were seeded (one cell per well) in 96-well plates. Clonal populations were expanded. ATM expression was then evaluated by immunoblot. Knockout (ATM-CL1–8), and control ($ATM^{wt}1$), clones were confirmed by immunostaining and Sanger sequencing after TA Topo cloning. $ATM^{wt}2$ was generated as another control after transfection of a control CRISPR/Cas9 plasmid (sc-418922).

#### 2.4.3. Cell viability assays

Cells were seeded into 96-well plates (1500 for PC3 and DU-145 and 2500 for LNCaP and 22Rv1) and treated the following day with the drug of interest or vehicle; 6 d later, the cells were stained with Annexin V-FITC and propidium iodide following manufacturer's instructions (eBioscience Annexin V-FITC Apoptosis Detection Kit; Thermo Fisher). Data were acquired with a Becton-Dickinson FACS Celesta flow cytometer and analysed using the FlowJo software.

#### 2.4.4. Immunofluorescence

Immunofluorescence was performed for RAD51, γH2AX, and 53BP1; image acquisition used the IN-Cell Analyzer 2000 (GE Healthcare). Multiple fields within a well were acquired to include a minimum of 1000 cells per sample-well. High content analysis of the images was processed using the IN-Cell Investigator 2.7.3 software [23]. Further details are provided in the Supplementary material.

#### 2.4.5. DR-GFP reporter plasmids

The 22Rv1 cells were seeded and transfected after 24 h with 3 μg of the pHPRT-DR-GFP vector (Addgene 26475) using a TransIT-X2 reagent (Myrus); 48 h later, puromycin (1 μg/ml) was added to the media for 4 d. Surviving cells (22Rv.1-DR-GFP stable line) were seeded onto 96-well plates (4000 cells per well) and treated with drugs of interest or vehicle for 24 h. The following day, an SceI endonuclease expression vector (Addgene 26477) was transfected (100 ng per well) using a TransIT-X2 reagent (Myrus). GFP-positive cells were analysed in a Becton-Dickinson FACS Celesta flow cytometer 48 h after SceI expressing vector transfection. A pBabe Cherry vector was used as a transfection control, and results across clones were normalised according to the percentage of $Cherry^{+}$ cells.

### 2.5. Patient-derived xenograft and organoid experiments

The castrated subline CP50C of the ATM loss patient–derived tumour model CP50 was used to generate organoid cultures for in vitro testing and for in vivo studies, as described previously [24]. The methods are provided in the Supplementary material.

## 3. Results

### 3.1. ATM IHC, NGS, and genomic instability

ATM IHC was performed on 800 samples from 653 patients (Fig. 1A and Supplementary Fig. 1), with 766 samples from 631 patients being evaluable; 68/631 (11%) patients had ATM loss. Overall, 102 patients had both diagnostic hormone-sensitive PC (HSPC) and CRPC samples tested for ATM IHC. Synchronous and metachronous, intra- and interpatient heterogeneity in ATM loss was observed (Fig. 1B–F); a patient was deemed to have ATM loss disease if at least one biopsy demonstrated this. ATM IHC status was often unchanged in matching, same-patient ($n = 102$) HSPC and CRPC, although in five patients, one sample was negative for ATM IHC and another sample had weak but positive staining (Fig. 1E and 1F). Population characteristics are listed in Supplementary Table 6; median overall survival from diagnosis for the ATM loss cohort (ATM IHC score 0) was 76 mo (95% CI: [67.4; 99]), with a median time from diagnosis to CRPC of 19.6 mo (95% CI: [17.2; 26]); median overall survival from CRPC was 50.9 mo (95% CI: [47.9; 65.8]). None of these were significantly different from the control population (positive ATM IHC) in univariate analysis (Fig. 2).

In 552 patients (621 samples), both IHC and NGS data were available. The prevalence of ATM pathogenic mutations (defined as the proportion of patients with at least a frameshift indel, a mutation resulting in a stop gain, splice site mutations, missense mutations in the kinase domain previously described as likely pathogenic, or homozygous deletions) was 37/552 (6.7%); eight patients (five with ATM IHC loss; three with no ATM loss) had two contemporaneous pathogenic mutations in a single biopsy. ATM loss by IHC in this set was 61/552 (11%). Overall, 24/61 patients with complete ATM loss by IHC had one or more pathogenic mutations, including two with ATM homozygous deletions; in 14 cases, a shallow ATM copy loss was detected (Fig. 3A). Interestingly, 23/61 patients (39%; 25 samples from 23 patients) had ATM protein loss by IHC, but no gene alterations were detected by targeted sequencing. In 48/496 (9.7%; 55 samples from 48 patients) PCs with no ATM IHC loss detected, *ATM* gene alterations were identified, but most of these were missense mutations of uncertain significance, although 13/496 (2.6%) patients had a mutation either truncating or in the kinase domain (Fig. 3B). Detected mutations in HSPC and CRPC samples are presented in Supplementary Fig. 2 and Supplementary Table 6.

WES was available for 79 CRPC biopsies for which we had ATM IHC (17 ATM loss, 52 ATM WT and BRCA WT, and 10 BRCA mutated). ATM loss tumours had evidence of increased genomic instability including higher burdens of telomeric allelic imbalance (NtAI: median 25 vs 18.5, Student *t* test $p = 0.005$) and large-scale transitions (LSTs: median 25 vs 19.5, Student *t* test $p = 0.048$; Fig. 3C and 3D).

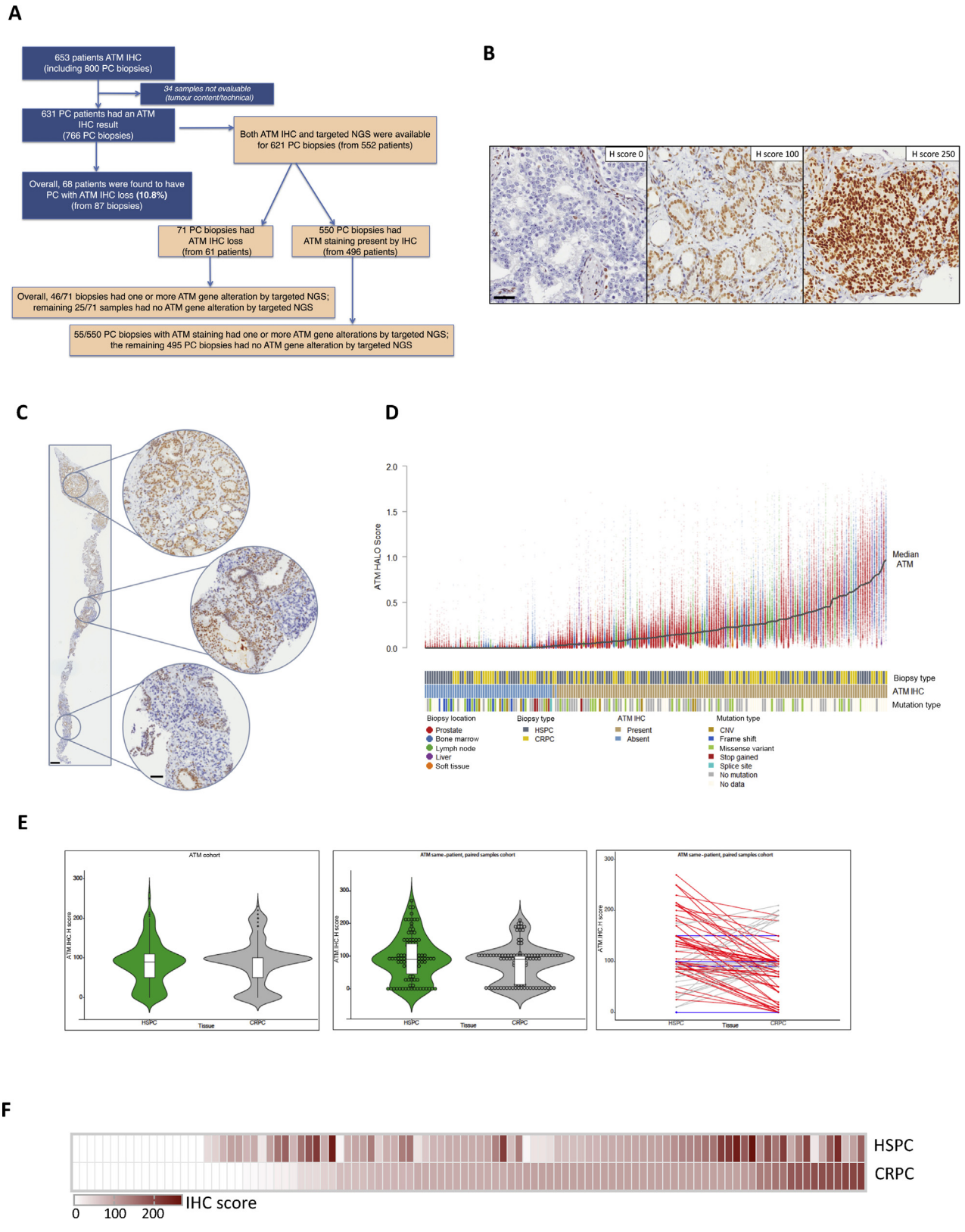


**Fig. 1 – Landscape of ATM expression in advanced prostate cancer. (A) A CONSORT diagram representing study population disposition. (B) Representative micrographs, and corresponding H scores, of ATM IHC in prostate cancer biopsies (20× magnification; scale bar represents 100 μm). (C) Representative examples of ATM IHC intrapatient heterogeneity within the same biopsy. (D) Scatterplot illustration correlating intra- and interpatient heterogeneity in same-patient biopsy samples with the degree of heterogeneity in PC without ATM loss, depicting heterogeneity in ATM protein expression within each sample as measured by Shannon's diversity index (SDI) and depicted as bar charts (lower panel). Colour dots represent visual scores per cell generated by a trained Halo AI supervised machine learning algorithm (HALO AI; Indica Labs, NM, USA; upper panel), with colours indicating origin of biopsy tissue as indicated by the legend. (E) Violin plots representing the H scores in the overall study population (left; divided as hormone-naïve and castration-resistant biopsies, compared using Wilcoxon test, $p = 0.4$); the subpopulation with matched, same-patient, hormone-naïve, and castration-resistant biopsies (centre;**

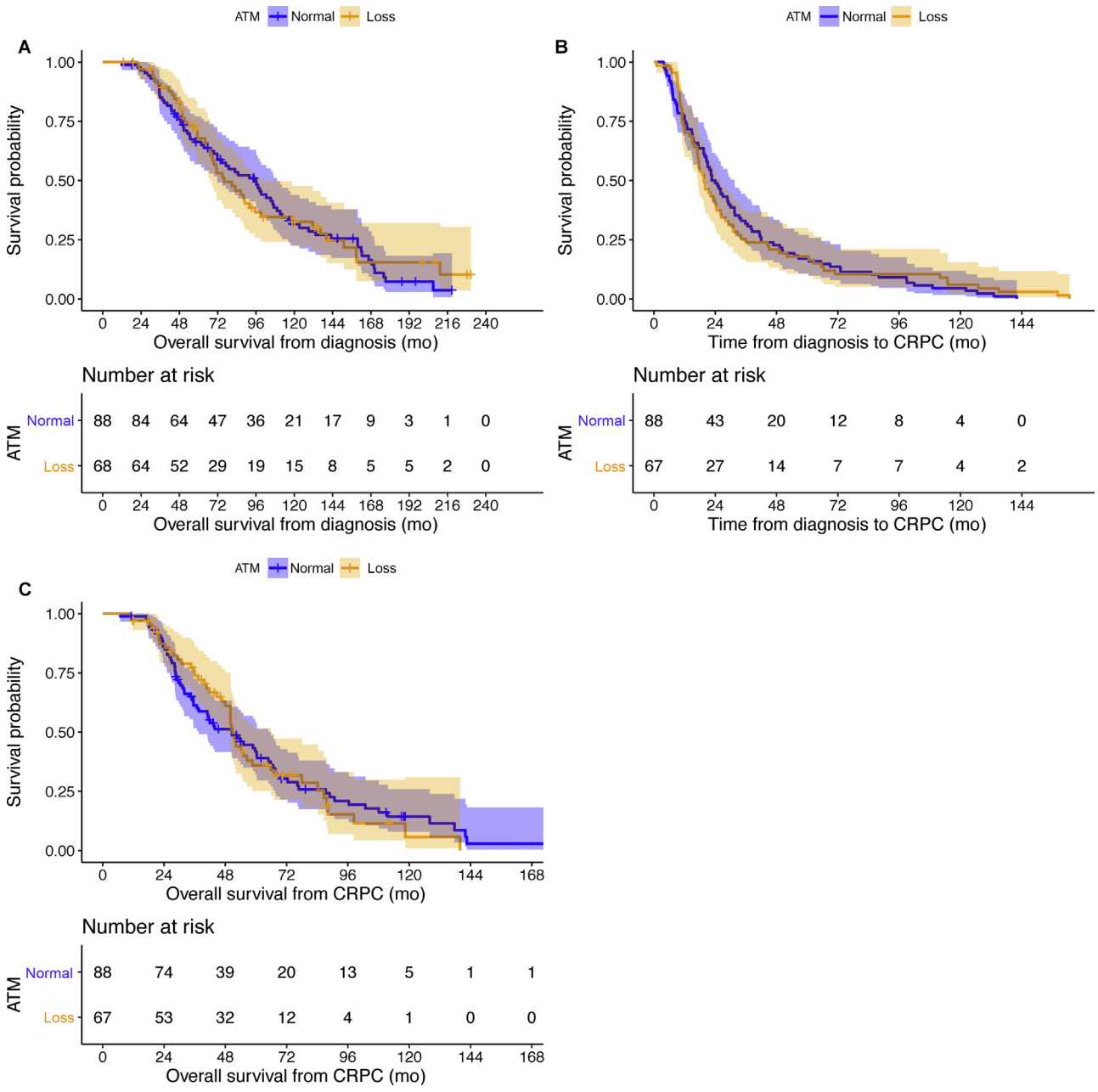


**Fig. 2 – ATM loss and clinical outcome data. Kaplan-Meier curves by ATM status for (A) overall survival from diagnosis (log rank $p = 0.8$), (B) time from diagnosis to CRPC (log rank $p = 1.0$), and (C) overall survival from mCRPC (log rank $p = 0.9$).**
**CRPC = castration-resistant prostate cancer; mCRPC = metastatic castration-resistant prostate cancer.**

### 3.2. *ATM knockout and PARP and ATR inhibition in PC cell lines*

Next, we investigated ATM deletion by CRISPR/Cas9-mediated stable elimination of ATM in 22Rv.1 cells. ATM loss was confirmed by immunoblotting for ATM and CHK2 (T68) phosphorylation (Supplementary Fig. 3A and 3B). Surprisingly, different sensitivities to PARP inhibition were observed in some of the ATM CRISPR clones when compared with the parental cell line and control CRISPR/Cas9 (ATMwt) cells (Fig. 4A and Supplementary Fig. 3). All ATM CRISPR clones presented biallelic truncating mutations, with the exception of the ATM-CL1, which had one frameshift and

**compared using Wilcoxon test, $p = 0.2$); and linear plots of the intrapatient change when comparing hormone-naïve and castration-resistant biopsies. (F) Heatmap illustrating H scores in matched, same-patient, HSPC, and CRPC biopsies. Scale bar indicates H scores correlated with colour intensity.**
**CNV = copy number variant; CRPC = castration-resistant prostate cancer; HSPC = hormone-sensitive prostate cancer; IHC = immunohistochemistry; *n* = number; NGS = next-generation sequencing; PC = prostate cancer.**

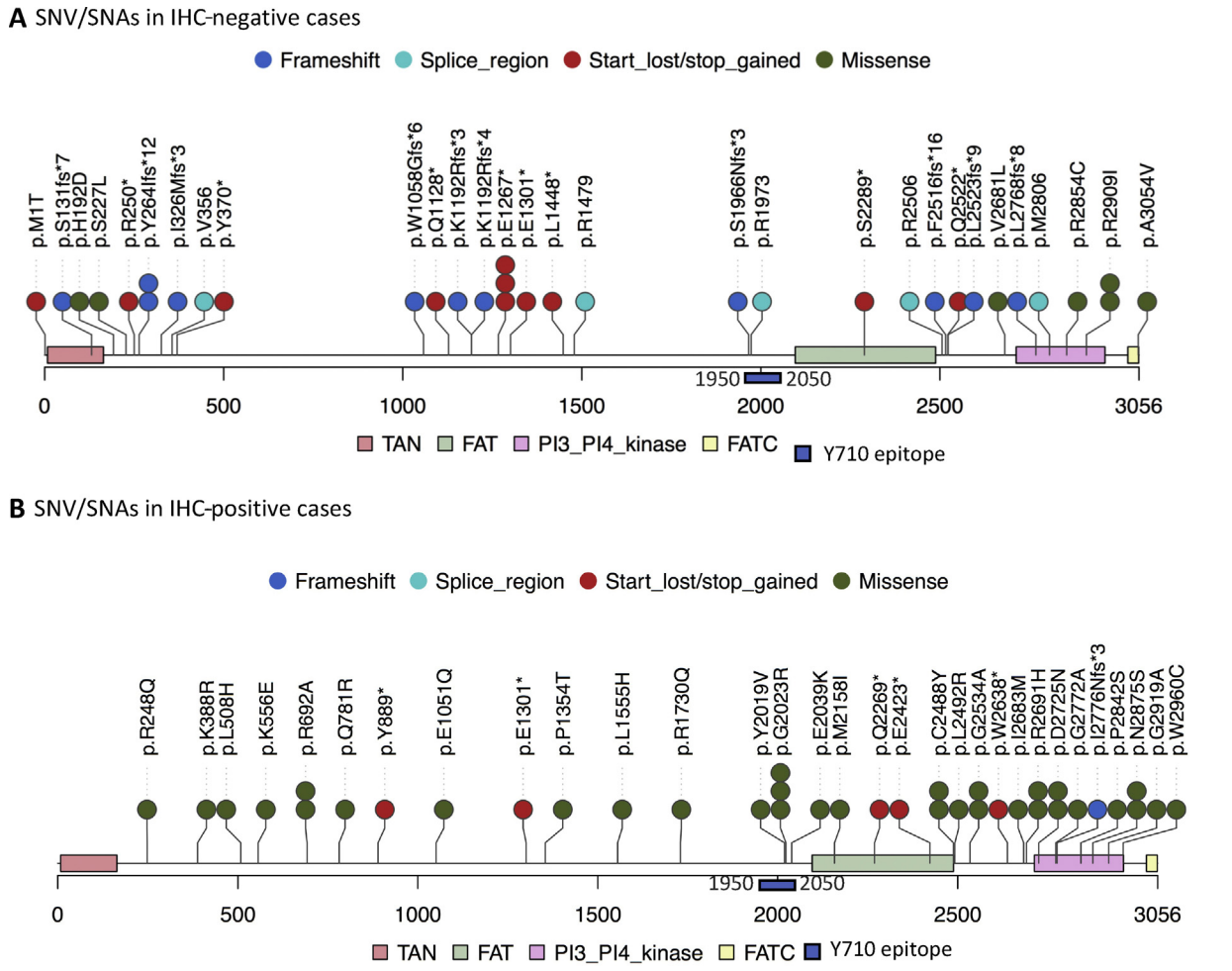


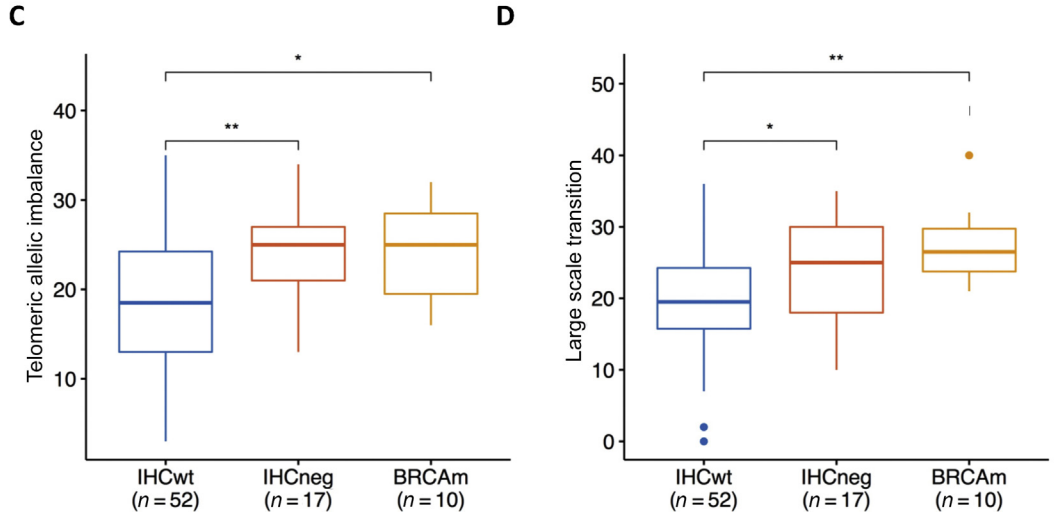


**Fig. 3 – Genomic characterisation of prostate cancers with and without loss of ATM expression. Lollipops representing the location and type of mutations found in the *ATM* gene in the study population in patient samples exhibiting (A) ATM loss (IHC score = 0) or (B) ATM positivity, by IHC (H score >0). The epitope against which the antihuman ATM antibody (Y710) binds is also depicted. (C and D) Analyses of genomic instability in a subset of the study population with whole-exome sequencing data, based on accumulation of large-scale transitions and burden of telomeric imbalances (NtAI) for patients with ATM loss by IHC ($n = 17$), ATM-WT and BRCA-WT ($n = 52$), and BRCA-mut ($n = 10$) tumours. Student $t$ test was used to calculate the $p$ values with *** $p \leq 0.001$, ** $p \leq 0.005$, and * $p \leq 0.05$.**
**IHC = immunohistochemistry; NtAI = number of subchromosomal regions with allelic imbalance extending to the telomere.**

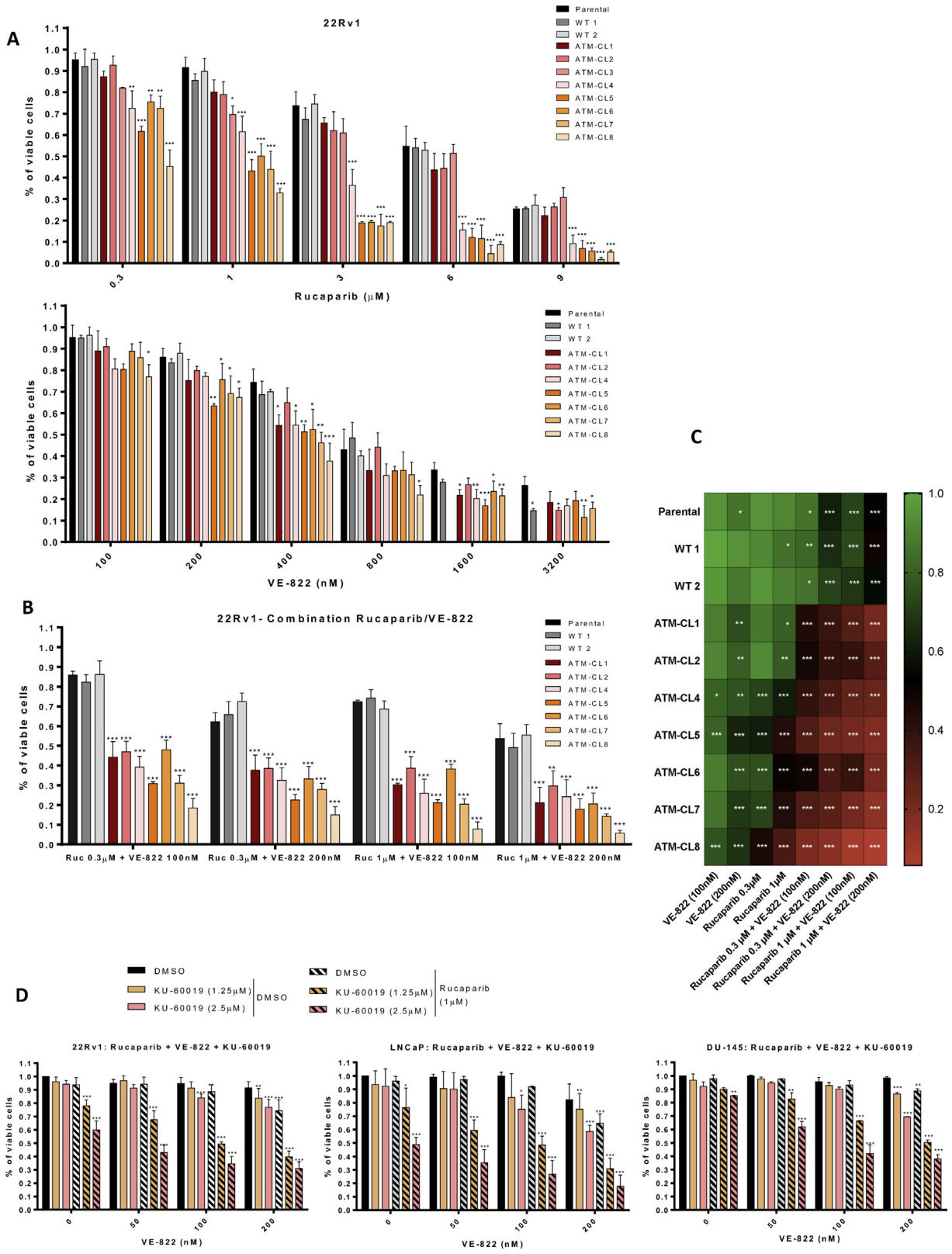


**Fig. 4 – ATM loss and sensitivity to PARP and ATR inhibitors as single agents or in combination in prostate cancer cell line models. The 22Rv1 cells were treated for 6 d with (A) the indicated doses of rucaparib (upper panel), ATR inhibitor (VE-822; bottom panel), or (B) a combination of both ($n = 3$). The models tested included the parental cell line, eight different clones with loss of ATM expression after CRISPR (ATM-CL1–8), and two additional controls: an ATM-WT clone after unsuccessful ATM CRISPR (WT1) and an ATM-WT clone manipulated following the same CRISPR protocol but without ATM guide (WT2). All Western blots for ATM expression are presented in the Supplementary material. Cell viability was measured based on the percentage of cells negative for both annexin V and PI staining. Statistical tests compared each clone with the parental cell line. (C) Heatmaps depicting enhanced sensitivity of ATM-deficient models to dual PARP-ATR inhibition. Statistical tests compare each clone with each untreated model ($n = 3$). (D) Bar plots reflecting the effect of combined PARP-ATM-ATR inhibition in 22Rv1 ($n = 4$), LNCaP ($n = 4$), and DU-145 ($n = 2$) parental cell lines;**

one in-frame deletion and no sensitivity to PARP inhibitors (Supplementary Fig. 3F and 3G, and Supplementary Table 7). Sensitivity of ATM CRISPR clones to cisplatin paralleled PARP inhibitor sensitivity, whereas all ATM CRISPR clones were sensitive to radiation (Supplementary Fig. 3D and 3E). We also investigated the effect of ATR inhibition alone, or in combination with PARP inhibition, in these ATM CRISPR models. Unlike PARP inhibition, ATR inhibition with both VE-822 and BAY-1895344 had a mild but consistent cytotoxic effect across all the ATM CRISPR clones (Fig. 4A and Supplementary Fig. 4B). Combined ATR and PARP inhibition had a synergistic interaction across all the ATM CRISPR clones, regardless of baseline sensitivity to PARP inhibition (Fig. 4B and 4C, and Supplementary Fig. 4C, 4D, and 5). To support these findings, we assessed the effect of combining ATR and PARP inhibition with the ATM inhibitor KU-60019 in multiple PC cell lines (22Rv1, LNCaP, and DU-145). The specificity of these inhibitors was confirmed by selective impairment of CHK2 T68 and CHK1 S345 phosphorylation, respectively (Supplementary Fig. 4A). In all tested cell lines, ATM-PARP and ATM-ATR inhibition combinations resulted in moderate cytotoxicity, while combined PARP and ATR inhibition with ATM kinase blockade had significantly superior antitumour activity (Fig. 4D).

### 3.3. A patient-derived model with ATM loss and PARP and ATR inhibition

We next analysed these anticancer drugs in a patient-derived xenograft (PDX) acquired from an mCRPC patient with ATM loss by IHC and sequencing in archival and preimplantation biopsy (Supplementary Fig. 6A). This model (CP50) also has AR and AKT2 amplification. The patient had received abiraterone, enzalutamide, docetaxel, and cabazitaxel, after which he had a lymph node biopsy that led to this PDX, prior to receiving olaparib to which he did not respond (Fig. 5A) [24]. ATR, CHK1, CHK2, and KAP as well as AR and AR splice variants increase with castration (CP50C) in vivo, with this being wildtype for TP53, PTEN, and MYC (Fig. 5B and Supplementary Fig. 6) [24]. In keeping with this patient's lack of response, in vitro CP50C organoid cultures were resistant to olaparib. ATR inhibition, however, exhibited antitumour activity in the nanomolar range, with this being enhanced by combined PARP and ATR inhibition (Fig. 5C and 5D).

These results were confirmed in in vivo studies. We implanted CP50C into castrated animals; tumours were allowed to grow to 200 $mm^3$ and then treated with the ATR inhibitor BAY1895344 and olaparib, or both (Supplementary Fig. 6). In vivo, CP50C was resistant to PARP inhibition and responded to ATR inhibition at 50 mg/kg (Supplementary Fig. 6C), with combined PARP and ATR inhibition having superior antitumour activity (Fig. 5E and 5F).

### 3.4. ATM loss and homologous recombination DNA repair function

We also studied DNA repair proficiency before and after ATM loss and drug treatment. First, we treated 22Rv.1 parental cells and ATM CRISPR and control clones with PARP inhibition alone, or in combination with ATR and ATM inhibitors. In an ATMwt context, PARP inhibition increased DNA DSBs with increased γH2AX and 53BP1 foci, these mostly colocalising with RAD51 foci, indicating activation of homologous recombination repair (HRR). When PARP was inhibited in ATM-deficient cells or with chemical inhibition of ATM, we observed reduced but not absent HRR with increased unresolved DSBs in keeping with ATM loss not causing a complete HRR defect, unlike BRCA2 loss. Conversely, when ATR function was inhibited in an ATM-KO background, loss of HRR was seen with complete loss of RAD51 foci induction, and increased γH2AX and 53BP1 foci accumulation (Fig. 6A and 6B, and Supplementary Fig. 7B). Similar results were observed in 22Rv11 ATM-WT cells and different PC lines when using the ATM inhibitor KU-60019 (Supplementary Fig. 7A and 7C).

To validate these results, we used a DR-GFP reporter assay, which allows measuring of HRR via transfection of a restriction endonuclease (I-SceI) to create DSBs in a GFP reporter cassette. Inhibition of ATM and ATR in 22Rv1 parental cells or ATR blockade in 22Rv1ATM CRISPR clones completely abolished the capacity of cells to repair I-SceI-induced DSBs by HRR, indicating that combined ATR and ATM blockade sensitises to PARP inhibition through HR loss and synthetic lethality (Fig. 6C). As HRR predominantly occurs during late S and early G2 cell cycle phases, we excluded the possibility that this loss of HRR was related to cells being unable to enter S/G2. Geminin staining, a biomarker of S-G2, showed that irrespective of HRR functionality, most damaged cells (50–80%) were in S/G2 (Supplementary Fig. 7D).

## 4. Discussion

Herein, we show that ATM IHC complete loss is found in >10% of advanced PCs and associates with genomic instability but not with complete loss of HRR function in preclinical ATM loss cell culture models, which showed variable PARP inhibitor sensitivity. Our data also indicate that targeted NGS does not detect all ATM loss and support comparing the predictive value of ATM IHC versus NGS in clinical studies of DNA repair targeting agents. In some cases, IHC loss may translate complex genomic

**22Rv1 (left), LNCaP (centre), and DU-145 (right) parental cell lines underwent treatment with the indicated doses of an ATM inhibitor (KU60019), with or without the ATR inhibitor (VE-822) and/or PARP inhibitor (rucaparib). The percentage of remaining viable cells was determined after 6 d based on negativity for both annexin V and PI staining. One-way ANOVA was used for all comparisons: *** $p < 0.001$, ** $p < 0.005$, and * $p < 0.05$. All error bars represent means ± SD; *n* represents the number of independent experiments.**
**ANOVA = analysis of variance; SD = standard deviation.**

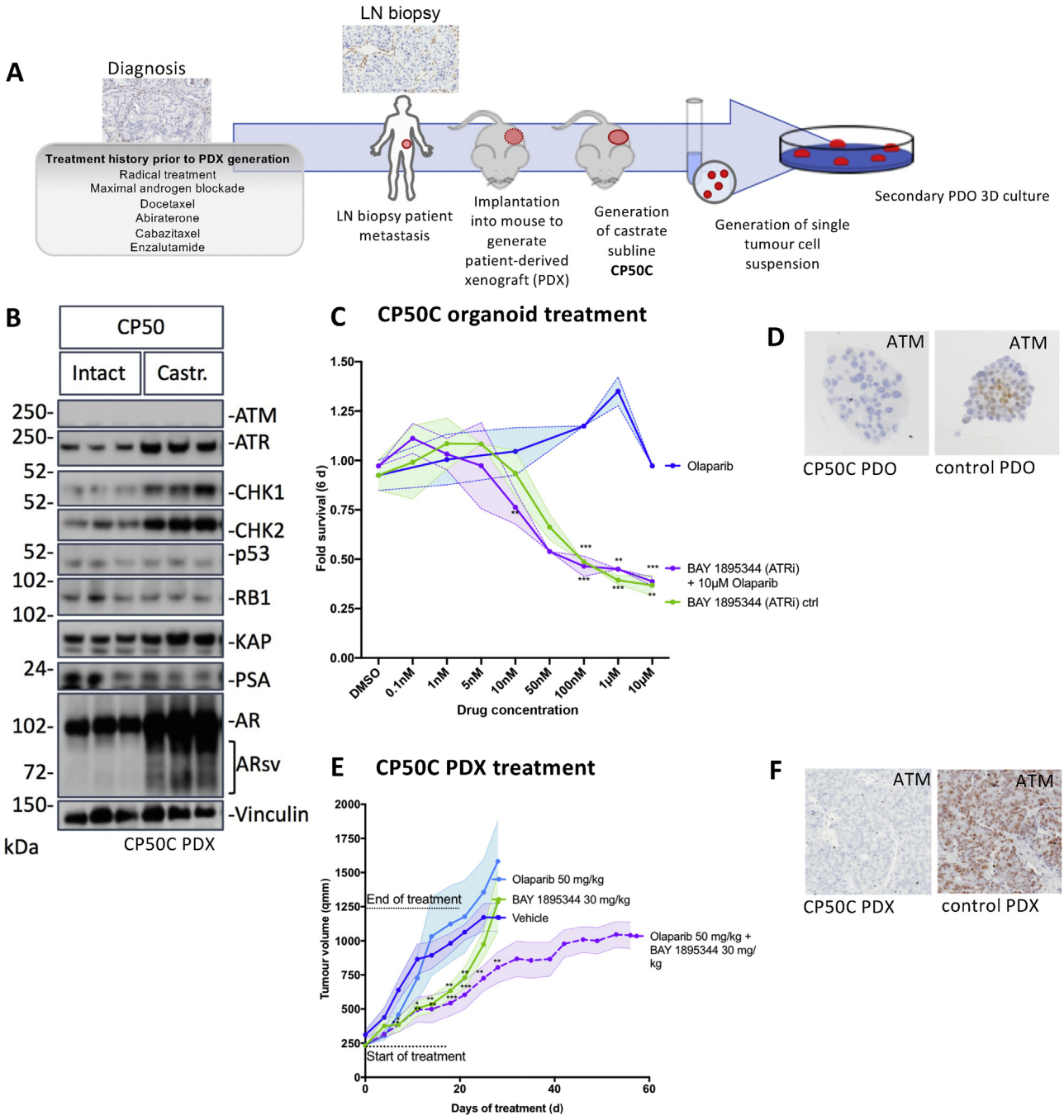


**Fig. 5 – ATR inhibition inhibits growth and sensitises to PARP inhibition, in an ATM loss, patient-derived, PC model. (A) Patient treatment history and the development of the ATM-negative, AR- and AKT2-amplified, PDX model CP50, and generation of organoid cultures from this model, are depicted. This patient's ATM immunohistochemistry at diagnosis and at mCRPC was 0, as depicted by the images, and his tumour did not have a response to olaparib clinically. (B) Western blot demonstrating ATM loss and upregulation of DNA damage repair proteins, upon castration in this model. (C) Organoid cultures generated from single cells, derived from castrated CP50 xenografts (CP50C), were treated with various concentrations of the ATR inhibitor BAY1895344 or the PARP inhibitor olaparib or the combination of BAY1895344 and 10 μM olaparib. Error shadows represent standard error; group size per arm is $n = 6$. All statistical tests are calculated using Student $t$ test: *** $p \leq 0.001$, ** $p \leq 0.005$, and * $p \leq 0.05$ against olaparib alone. (D) ATM IHC confirming the absence of ATM loss in CP50C PDX-derived organoids compared with ATM-proficient control PDO. (E) Castrated mice bearing CP50C were treated with either BAY 1895344 or olaparib, or BAY 1895344 with 10 μM olaparib. IC50 for BAY 1895344 single agent was 19.3 nM, whereas when used in combination with olaparib, the IC50 for BAY 1895344 was 2.4 nM. (F) ATM IHC confirming the absence of ATM loss in CP50C PDX tumours, compared with an ATM-proficient control PDX. Error shadows represent standard error; group size per arm is $n = 8$. All statistical tests are calculated using Student $t$ test: *** $p \leq 0.001$, ** $p \leq 0.005$, and * $p \leq 0.05$ against vehicle control.**
**ATRi = ATR inhibitor; Castr. = castrated; ctrl = control; IHC = immunohistochemistry; LN = lymph node; mCRPC = metastatic castration-resistant prostate cancer; PC = prostate cancer, PDO = patient-derived organoid; PDX = patient-derived xenograft.**

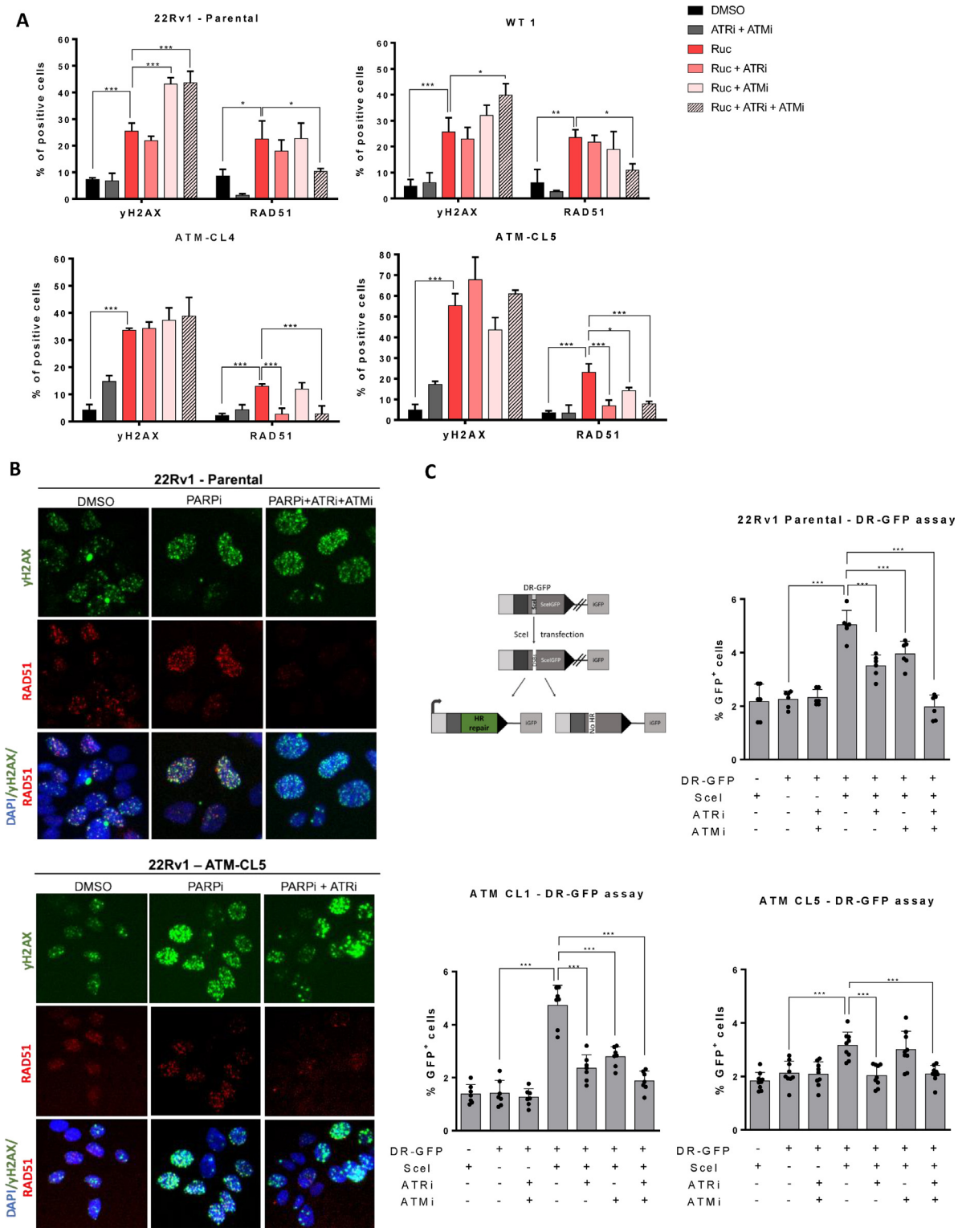


**Fig. 6 – Functional characterisation of prostate cancer cell line models suggests that HRR is suppressed only after blocking both ATM and ATR function. Quantification of the percentage of cells positive (more than five foci) for RAD51 and γH2AX ($n = 3$) immunofluorescence staining for 22Rv1 cell line models after treatment with 1 μM of rucaparib alone, or in combination with 2.5 μM of the ATMi KU-60019 and/or 200 nM of the ATRi VE-822 for 24 h. (A) Depicts HRR suppression in the 22Rv1 parental cell line, in an ATM-WT clone (wt1) only after concomitant ATM and ATR inhibition, and in ATM CRISPR clones (ATM-CL4 and ATM-CL5), where ATR inhibition results in HRR suppression. All statistical tests are calculated using one-way ANOVA: *** $p < 0.001$, ** $p < 0.005$, and * $p < 0.05$. All error bars represent means ± SD; $n$ represents the number of independent experiments. (B) Representative images of yH2AX and RAD51 immunofluorescence staining in the parental cell line and one of the ATM CRISPR clones are shown. (C) Validation of HR deficiency with the DRGFP assay upon ATM and ATR inhibition. The DR-GFP 22Rv1 parental, ATM-CL1, and ATM-CL5 cell lines (or original cells) were transfected with SceI enzyme alone, or in combination with 2.5 μM of the ATMi KU-60019 and/or 200 nM of the ATRi VE-822 for 48 h. The plot represents the percentage of GFP-positive cells quantified by FACS. All statistical tests are calculated using one-way ANOVA: *** $p < 0.001$, ** $p < 0.005$, and * $p < 0.05$. All error bars represent means ± SD. Dots represent independent experiments. ANOVA = analysis of variance; HRR = homologous recombination repair; SD = standard deviation.**

rearrangements or methylation that is not captured by targeted NGS assays being implemented in clinical practice. In others, discrepancies between IHC and NGS status may relate to the exact binding site of the antibody compared with the location of mutations within the large *ATM* gene, which may result in some proteins with late truncations being recognised by IHC. Moreover, studies are also needed to assess a relevant threshold for ATM IHC assays to guide patient stratification in clinical practice; in this study, we describe ATM loss as complete lack of expression (H score = 0), but several other cases in our cohort showed low ATM expression (H score between 5 and 30). While our clinical outcome analysis is limited by the number of patients and its retrospective nature, it is clear that patients with metastatic PC and ATM loss have poor prognosis and need novel therapeutic approaches. In our study, we show that ATR inhibition has consistent antitumour activity against ATM loss PC models, unlike PARP inhibition, with the combination having superior activity to either one alone, probably due to ATR inhibition in an ATM loss context resulting in supressed HRR.

Previous laboratory and clinical studies indicate that ATM loss does not result in HRR defects; multiple silencing RNA screens show that ATM loss can be synthetically lethal with PARP inhibition, although this may be tumour background dependent [28]. Rafiei et al [17] recently reported poor sensitivity to PARP inhibitors in ATMko PC cell lines with sensitivity to single-agent ATR inhibitors. Our data mirror clinical experience, with ATM loss sensitising in some but not all derived clones, suggesting that this synthetic lethality is background dependent and sensitive models still presented RAD51 foci. Further studies of the molecular events co-occurring with ATM loss are needed to elucidate determinants of PARP inhibitor sensitivity in ATM loss PC. Nonetheless, our studies herein indicate that combined PARP and ATR inhibition merits clinical trial evaluation in ATM-deficient PC and may be superior to either ATR or PARP inhibition alone, although careful dose- and schedule-finding phase 1 trials will be needed since both these drug classes cause haematological toxicity.

Our study has multiple limitations, one of which is the availability of clinical data for only a proportion of our overall population. Another limitation of our study is that some of our data were generated in clones derived from 22Rv.1, a PC cell line with an underlying DNA repair defect but preserved baseline HRR and resistant to the drugs tested. These results were, moreover, replicated in several PC models using ATM inhibitors and in an ATM loss patient–derived model.

## 5. Conclusions

ATM loss defines a distinct PC subtype, characterised by increased genomic instability, with variable sensitivity to PARP inhibition, sensitivity to ATR inhibition, and most sensitivity to combined inhibition, which now merits clinical evaluation.

***Author contributions:*** Joaquin Mateo had full access to all the data in the study and takes responsibility for the integrity of the data and the accuracy of the data analysis.
*Study concept and design*: Neeb, Herranz, Carreira, Mateo, de Bono.
*Acquisition of data*: Neeb, Herranz, Arce-Gallego, Miranda, Buroni, Yuan, Athie, Casals, Carmichael, Nava Rodrigues, Gurel, Rescigno, Casanova-Salas, Cordoba, Fenor de la Maza, Seed, Chandran, Ferreira, Figueiredo, Bertan, Bianchini, Aversa, Paschalis, Gonzalez, Morales-Barrera, Suarez, Carles, Sharp.
*Analysis and interpretation of data*: Neeb, Herranz, Arce-Gallego, Yuan, Athie, V. Gil, J. Gil, Serra, Lord, Carreira, Mateo, de Bono.
*Drafting of the manuscript*: Neeb, Herranz, Arce-Gallego.
*Critical revision of the manuscript for important intellectual content*: All authors.
*Statistical analysis*: Rekowski, Yuan.
*Obtaining funding*: Mateo, de Bono.
*Administrative, technical, or material support*: None.
*Supervision*: Carreira, Mateo, de Bono.
*Other*: None.

***Financial disclosures:*** Joaquin Mateo certifies that all conflicts of interest, including specific financial interests and relationships and affiliations relevant to the subject matter or materials discussed in the manuscript (eg, employment/affiliation, grants or funding, consultancies, honoraria, stock ownership or options, expert testimony, royalties, or patents filed, received, or pending), are the following: J. Gil has acted as a consultant for Unity Biotechnology, Geras Bio, and Merck KGaA; and owns equity in Unity Biotechnology and Geras Bio. J. Gil and N. Herranz are named inventors in an MRC patent related to senolytic therapies (no related to this work). R. Morales-Barrera reports a consulting or advisory role for and/or a role in the speakers' bureaus of Sanofi Aventis, Bayer, Janssen, AstraZeneca, Merck Sharp & Dohme, and Asofarma; and received travel and accommodations expenses from Roche, Sanofi Aventis, Astellas, Janssen, Merck Sharp & Dohme, Bayer, Pharmacyclics, Clovis Oncology, and Lilly. J. Carles has served on the advisory boards of Bayer, Johnson & Johnson, BMS, Astellas, Pfizer Oncology, Sanofi, MSD, Rocher, and AstraZeneca; has participated in speakers' bureaus of Bayer, Johnson & Johnson, Asofarma, and Astellas; has received support for travel to conference from BMS, Ipsen, Roche, and AstraZeneca; and is the PI of several industry-sponsored clinical trials. J. Mateo has served on advisory boards of Amgen, AstraZeneca, Clovis Oncology, Janssen, Merck/MSD, and Roche; has received research funding from AstraZeneca and Pfizer Oncology (not related to this work); and is the PI of several industry-sponsored clinical trials. J. de Bono has served on advisory boards of and received fees from many companies including Astra Zeneca, Astellas, Bayer, Bioxcel Therapeutics, Boehringer Ingelheim, Cellcentric, Daiichi, Eisai, Genentech/Roche, Genmab, GSK, Janssen, Merck Serono, Merck Sharp & Dohme, Menarini/Silicon Biosystems, Orion, Pfizer, Qiagen, Sanofi Aventis, Sierra Oncology, Taiho, and Vertex Pharmaceuticals; is an employee of The ICR, which have received funding or other support for his research work from AZ, Astellas, Bayer, Cellcentric, Daiichi, Genentech, Genmab, GSK, Janssen, Merck Serono, MSD, Menarini/Silicon Biosystems, Orion, Sanofi Aventis, Sierra Oncology, Taiho, Pfizer, and Vertex, and which has a commercial interest in abiraterone, PARP inhibition in DNA repair defective cancers, and PI3K/AKT pathway inhibitors (no personal income); was named an inventor, with no financial interest, for patent 8,822,438; and has been the CI/PI of many industry-sponsored clinical trials. All other authors declare no relevant conflicts of interest.

***Funding/Support and role of the sponsor*:** We gratefully acknowledge research funding for this work from Cancer Research UK, Prostate Cancer UK, the Movember Foundation through the London Movember Centre of Excellence (CEO13_2-002), the Prostate Cancer Foundation (including Young Investigator Awards to Joaquin Mateo, Pasquale Rescigno, and

Adam Sharp), Stand Up To Cancer, an d the UK Department of Health through an Experimental Cancer Medicine Centre grant. Professor Johann de Bono is a National Institute for Health Research (NIHR) Senior Investigator; research at the Royal Marsden Hospital is supported by a Biomedical Research Centre grant. Part of this work was also funded by Instituto de Salud Carlos III through Grant FI19/00280 to Sara Arce-Gallego, Grant CP19/00170 to Nicolas Herranz, and Grant PI18/01384 to Joaquin Mateo. The authors affiliated to VHIO acknowledge the "la Caixa" Foundation (ID 100010434) for funding under agreement LCF/PR/PR17/51120011 and funding from Fundacion FERO and Moventia. This project has received funding from the European Union's Horizon 2020 research and innovation programme under the Marie Skłodowska-Curie grant agreement 837900. The funding organisations had no role in the design, conduction or data analysis of this project, neither in the manuscript preparation.

***Acknowledgements*:** The authors affiliated to VHIO acknowledge the Cellex Foundation for providing research facilities and equipment. We thank Dr Marcos Malumbres at the Spanish National Cancer Research Center (CNIO) for providing the DR-GFP plasmid.

## Uncited references

[25,26,27].

## Appendix A. Supplementary data

Supplementary material related to this article can be found, in the online version, at doi:https://doi.org/10.1016/j.eururo.2020.10.029.

## References

[1] Abida W, Cyrta J, Heller G, et al. Genomic correlates of clinical outcome in advanced prostate cancer. Proc Natl Acad Sci U S A 2019;116:11428–36.
[2] Armenia J, Wankowicz SAM, Liu D, et al. The long tail of oncogenic drivers in prostate cancer. Nat Genet 2018;50:645–51.
[3] Robinson D, Van Allen EM, Wu YM, et al. Integrative clinical genomics of advanced prostate cancer. Cell 2015;162:454.
[4] de Bono J, Mateo J, Fizazi K, et al. Olaparib for metastatic castration-resistant prostate cancer. N Engl J Med 2020;382:2091–102.
[5] Mateo J, Porta N, Bianchini D, et al. Olaparib in patients with metastatic castration-resistant prostate cancer with DNA repair gene aberrations (TOPARP-B): a multicentre, open-label, randomised, phase 2 trial. Lancet Oncol 2020;21:162–74.
[6] Abida W, Campbell D, Patnaik A, et al. Non-BRCA DNA damage repair gene alterations and response to the PARP inhibitor rucaparib in metastatic castration-resistant prostate cancer: analysis from the phase 2 TRITON2 study. Clin Cancer Res 2020;26:2487–96.
[7] Lang SH, Swift SL, White H, Misso K, Kleijnen J, Quek RGW. A systematic review of the prevalence of DNA damage response gene mutations in prostate cancer. Int J Oncol 2019;55:597–616.
[8] Robinson D, Van Allen EM, Wu YM, et al. Integrative clinical genomics of advanced prostate cancer. Cell 2015;161:1215–28.
[9] Antonarakis ES, Lu C, Luber B, et al. Germline DNA-repair gene mutations and outcomes in men with metastatic castration-resistant prostate cancer receiving first-line abiraterone and enzalutamide. Eur Urol 2018;74:218–25.
[10] Shiloh Y. ATM and related protein kinases: safeguarding genome integrity. Nat Rev Cancer 2003;3:155–68.
[11] Blackford AN, Jackson SP. ATM, ATR, and DNA-PK: the trinity at the heart of the DNA damage response. Mol Cell 2017;66:801–17.
[12] Yoo HY, Kumagai A, Shevchenko A, Shevchenko A, Dunphy WG. Ataxia-telangiectasia mutated (ATM)-dependent activation of ATR occurs through phosphorylation of TopBP1 by ATM. J Biol Chem 2007;282:17501–6.
[13] Zeman MK, Cimprich KA. Causes and consequences of replication stress. Nat Cell Biol 2014;16:2–9.
[14] Toledo LI, Altmeyer M, Rask MB, et al. ATR prohibits replication catastrophe by preventing global exhaustion of RPA. Cell 2013;155:1088–103.
[15] Couch FB, Bansbach CE, Driscoll R, et al. ATR phosphorylates SMARCAL1 to prevent replication fork collapse. Genes Dev 2013;27:1610–23.
[16] Vakifahmetoglu H, Olsson M, Zhivotovsky B. Death through a tragedy: mitotic catastrophe. Cell Death Differ 2008;15:1153–62.
[17] Rafiei S, Fitzpatrick K, Liu D, et al. ATM loss confers greater sensitivity to ATR inhibition than PARP inhibition in prostate cancer. Cancer Res 2020;80:2094–100.
[18] Min A, Im SA, Jang H, et al. AZD6738, A novel oral inhibitor of ATR, induces synthetic lethality with ATM deficiency in gastric cancer cells. Mol Cancer Ther 2017;16:566–77.
[19] Sharp A, Coleman I, Yuan W, et al. Androgen receptor splice variant-7 expression emerges with castration resistance in prostate cancer. J Clin Invest 2019;129:192–208.
[20] Sundar R, Miranda S, Rodrigues DN, et al. Ataxia telangiectasia mutated protein loss and benefit from oxaliplatin-based chemotherapy in colorectal cancer. Clin Colorectal Cancer 2018;17:280–4.
[21] Mateo J, Carreira S, Sandhu S, et al. DNA-repair defects and olaparib in metastatic prostate cancer. N Engl J Med 2015;373:1697–708.
[22] Birkbak NJ, Wang ZC, Kim JY, et al. Telomeric allelic imbalance indicates defective DNA repair and sensitivity to DNA-damaging agents. Cancer Discov 2012;2:366–75.
[23] Herranz N, Gallage S, Mellone M, et al. mTOR regulates MAPKAPK2 translation to control the senescence-associated secretory phenotype. Nat Cell Biol 2015;17:1205–17.
[24] Welti J, Sharp A, Yuan W, et al. Targeting bromodomain and extra-terminal (BET) family proteins in castration-resistant prostate cancer (CRPC). Clin Cancer Res 2018;24:3149–62.
[25] Yip S, Khalaf D, Struss WJ, et al. Outcomes in patients (Pts) with advanced prostate cancer and inactivating germline mutations in BRCA2 or ATM. J Clin Oncol 2018;36(6_suppl):242.
[26] Carter HB, Helfand B, Mamawala M, et al. Germline mutations in ATM and BRCA1/2 are associated with grade reclassification in men on active surveillance for prostate cancer. Eur Urol 2019;75:743–9.
[27] Mohni KN, Thompson PS, Luzwick JW, et al. A synthetic lethal screen identifies DNA repair pathways that sensitize cancer cells to combined ATR inhibition and cisplatin treatments. PLoS One 2015;10:e0125482.